



Full length article

Effect of heterostructure and hetero-deformation induced hardening on the strength and ductility of brass

X.T. Fang^a, G.Z. He^{a,b}, C. Zheng^c, X.L. Ma^{d,*}, D. Kaoumi^e, Y.S. Li^f, Y.T. Zhu^{a,f,**}

^a Department of Materials Science and Engineering, North Carolina State University, Raleigh, NC 27695, USA

^b Department of Microsystems-IMS, Faculty of Technology, Natural Sciences and Maritime Sciences, University of South-Eastern Norway, Postboks 235, 3603 Kongsberg, Norway

^c Science and Technology on Thermostructural Composite Materials Laboratory, Northwestern Polytechnical University, Xi'an 710072, China

^d Department of Materials Science and Engineering, Texas A&M University, College Station, TX 77840, USA

^e Department of Nuclear Engineering, North Carolina State University, Raleigh, NC 27695, USA

^f Nano and Heterogeneous Structural Materials Center, School of Materials Science and Engineering, Nanjing University of Science and Technology, Nanjing 210094, China

ARTICLE INFO

Article History:

Received 11 August 2019

Revised 2 January 2020

Accepted 19 January 2020

Available online 22 January 2020

Keywords:

Heterogeneous structure

Geometrically necessary dislocation

Hetero-deformation induced hardening

ABSTRACT

Heterostructured materials have been reported to possess superior combinations of strength and ductility, which is attributed to hetero-deformation induced (HDI) strengthening and work hardening. However, the influence of heterostructural parameters on the evolution of HDI stress and mechanical behavior during tensile deformation is not well understood. In this paper, heterostructured brass (Cu–30%Zn) was fabricated by cold rolling and partial annealing, to produce heterostructures with different heterostructural parameters, including domain volume fraction, domain thickness/spacing and domain misorientation. It was found that HDI hardening was dominant when the tensile strain was less than ~4.5%, while conventional dislocation hardening became more effective at higher strain levels. Quick accumulation of geometrically necessary dislocations was found in the domain boundary regions, leading to high HDI stress. Higher domain misorientation was found more effective in developing HDI hardening. These findings elucidate the effect of heterostructure on strength and ductility, which can help with the design of heterostructured materials for superior mechanical properties.

© 2020 Acta Materialia Inc. Published by Elsevier Ltd. All rights reserved.

1. Introduction

Strength and ductility are two of the most important mechanical properties of metallic materials for structural applications in a wide variety of industries, including automobile and aerospace. For the last three decades, nanostructured and ultrafine-grained metals and alloys have been extensively studied to produce very high strength [1–7]. However, the high strength often comes at the sacrifice of ductility [8,9]. Low ductility means low tensile plasticity, which poses a safety issue for many structural applications. Developing metallic materials, with a good combination of strength and ductility, has been a challenge for researchers [10].

Recently, heterostructured materials containing both ultrafine- and coarse-grained domains have been reported to have a superior combination of strength and ductility [11,12]. Heterostructured materials are

defined as materials containing domains with dramatically different flow stresses [11,13,14]. Each domain can be an individual grain or a polycrystalline volume. According to the definition, several diverse groups of materials can be considered as heterostructured materials, including bimodal materials [15–17], gradient materials [18–21], heterogeneous lamella materials [11,22,23], harmonic structure [24–26], dual-phase steel [27–29], laminated materials [30–32], etc.

The common physics that links these very diverse microstructures is their ability to produce hetero-deformation induced (HDI) strengthening to enhance strength and HDI work hardening to retain ductility [30]. The HDI hardening was previously called back-stress hardening, which was found not accurate [14]. Specifically, the dramatically different flow stresses among adjacent domains lead to mechanical incompatibility during deformation. Before a sample yields as defined by 0.2% plastic strain, the soft domains are plastically deforming while the hard domains are still elastic. Dislocations gliding in the soft domains will be stopped and accumulated at the elastic/plastic domain boundaries. Some of these dislocations are likely emitted from Frank–Read dislocation sources, which have the same Burgers vector and can be defined as geometrically necessary dislocations (GNDs) [13]. The piling-up of GNDs is known to produce

* Corresponding author at: Department of Materials Science and Engineering, Texas A&M University, College Station, TX 77840, USA.

** Corresponding author at: Department of Materials Science and Engineering, North Carolina State University, Raleigh, NC 27695, USA.

E-mail addresses: xma4@ncsu.edu (X.L. Ma), ytzhu@ncsu.edu (Y.T. Zhu).

long-range internal stress, i.e., back stress in the soft domains, which makes the soft domains appear stronger. At the same time, the stress concentration at the head of the GND piling-up exerts strong forward stress in the adjacent hard domain. HDI stress is a combined effect of back stress and forward stress [14].

After yielding, there will be strain partitioning among the heterostructured domains, where the soft domain will be subjected to higher plastic strain than the hard domains [27]. Since the strain must be continuous, a plastic strain gradient will inevitably develop near the domain boundaries. It was believed that the plastic strain gradient has to be accommodated by GNDs [31,33], which leads to HDI hardening to retain or enhance ductility. However, it has been found recently that the accumulation of GNDs may not be proportional to the accumulation of plastic strain gradient [34].

Among all heterostructures, heterogeneous lamella structure (HLS) has been reported to produce the best combination of strength and ductility [11,13]. For example, the HLS Ti has been found to possess the high strength of ultrafine-grained Ti while maintaining the ductility of coarse-grained Ti [11], a combination that is deemed impossible according to conventional wisdom. However, it is also noteworthy that not all HLS materials are equally effective in improving the mechanical properties [22]. Thus, it is important to reveal the effects of different heterostructural parameters, including domain volume fraction, domain spacing/thickness, etc., on mechanical behaviors for achieving a superior combination of strength and ductility. Some progress has been made in understanding how the structural parameters influence the HDI stress evolution. Wu et al. [11] found that the volume fraction of soft domains should be less than 30% in Ti. Ma et al. [30] and Huang et al. [31] demonstrated that the optimal thickness of the soft domain was $\sim 15 \mu\text{m}$ in copper-brass (Cu10Zn) laminate materials. However, the microscopic evolution of GNDs, at the domain boundaries in HLS, has not been well explored. Specifically, it is not well understood how the structural parameters affect the evolution of GNDs and HDI stress in HLS materials.

In this study, HLS brass (Cu-30wt%) was fabricated by cold rolling combined with partial-recrystallization annealing. Since brass is a material with low stacking fault energy, dislocation cross-slip is hampered whereas pile-ups (GND) are promoted at the domain boundary. Microstructures at different tensile plastic strain levels were systematically analyzed to reveal the evolution of GNDs at the domain boundaries. Domain misorientation, a new parameter defined as the average misorientation between soft domains and hard domains, is found to affect the HDI-stress evolution and mechanical behavior.

2. Experiment

A commercial ASM-C26000 alloy (Cu-30 wt% Zn) plate was annealed at 700°C for 2 h to homogenize the sample (Fig. 1), producing a coarse-grained (CG) microstructure with an average grain size of several hundred micrometers. The CG plates were rolled (represented by “R”) from 10 mm to 2 mm (80% thickness reduction), with each pass producing $\sim 5\%$ thickness reduction. Subsequently, the rolled brass plate was annealed (“A”) at 260°C (“260C”) for 10 mins, 20 mins and 30 mins in a vacuum furnace.

Samples for ion channeling contrast microscopy (ICCM) and electron backscattered diffraction (EBSD) observation were firstly cut from the rolled and annealed samples, then mechanically polished to achieve a mirror-like surface. Electrochemical polishing was performed for <30 s to remove the strained top-surface layer. The electrolyte consisted of phosphoric acid (concentration of 85%), ethanol and deionized water with a volume ratio of 1:1:2. ICCM and EBSD were conducted in an FEI Quanta 3D FEG dual-beam instrument. For local misorientation mapping, each EBSD scan was performed under 30 kV and 16 nA electron beam and with a bin size of 2×2 to achieve a decent angular resolution [35,36].

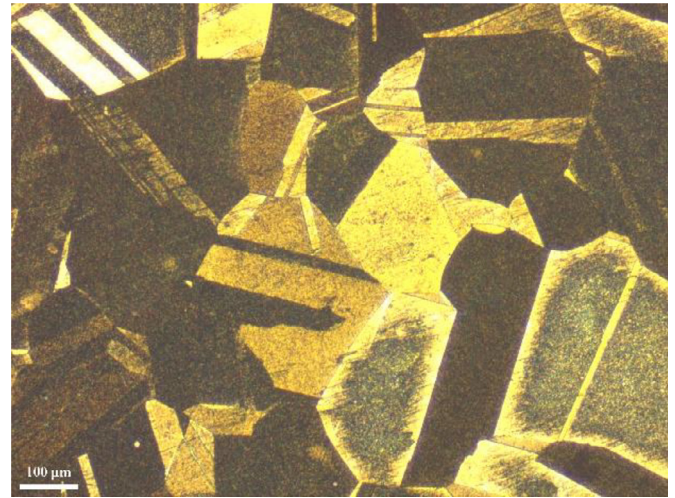


Fig. 1. Coarse-grained structure of brass (Cu-30wt%Zn) after annealing at 700°C for 2 h.

TEM foil was prepared by mechanically polishing the specimen to $100 \mu\text{m}$, followed by twin-jet polishing at -10°C . The electrolyte was the same as that for electrochemical polishing. TEM observation was performed in JEM-2000 and JEM-2010F microscopes operating at 200 kV.

Dog-bone-shaped tensile samples with gauge dimensions of $10 \times 2 \times 2 \text{ mm}^3$ were tested under uniaxial tension on a Shimadzu AGS machine. Both normal and unloading-reloading tension tests were carried out at room temperature at a strain rate of $5 \times 10^{-4} \text{ s}^{-1}$, and each test was repeated for at least 5 samples to ensure data reproducibility. X-ray diffraction (XRD) was conducted on well-polished tensile samples with a Cu $K\alpha$ radiation source. The dislocation density analysis was based on the Williamson-Hall equation, and the details of the method could be found in Refs [37,38].

3. Results

3.1. Structural characterization

The global microstructure of rolled and annealed samples was observed by using ion channeling contrast microscopy (ICCM), as shown in Fig. 2. After partial-recrystallization annealing for 10–30 mins, three different heterogeneous lamella structures (HLS) were obtained. As shown in Fig. 2(a), 80% rolling reduction produced ultrafine grains in brass. The as-rolled structure contains a high density of dislocation cells and low-angle boundaries [39,40], which is further detailed in Fig. S1. During annealing, recovery occurred first to decrease dislocation density in each lamella domain without changing its morphology [41,42]. Subsequently, new grains were nucleated in colonies. Since the nucleation of the new grains is not simultaneous and the growth rates of the new grains are different, the sizes of the new grains vary significantly [43]. This produced two types of domains, soft domains and hard domains. Soft domains are aggregations of fully recrystallized coarse grains, whose grain sizes are larger than $1 \mu\text{m}$, while hard domains are aggregations of ultrafine grains either from severe deformation or limited recrystallization. Because the flow stresses of the soft domain and hard domain are different during deformation, HDI stress will develop in the heterostructured sample, which may lead to high strength and ductility in HLS materials [10].

TEM images of hard and soft domains in the R80_A260C_20 min sample are shown in Fig. 3. Fig. 3(a) shows the microstructure inside a hard domain, which consists of both equiaxed and elongated ultrafine grains with sizes ranging from $\sim 100 \text{ nm}$ to $\sim 600 \text{ nm}$. Fig. 3(b) shows the recrystallized grains inside a soft domain, with grain sizes ranging from $\sim 2 \mu\text{m}$ to $\sim 8 \mu\text{m}$. The recrystallized coarse grains often

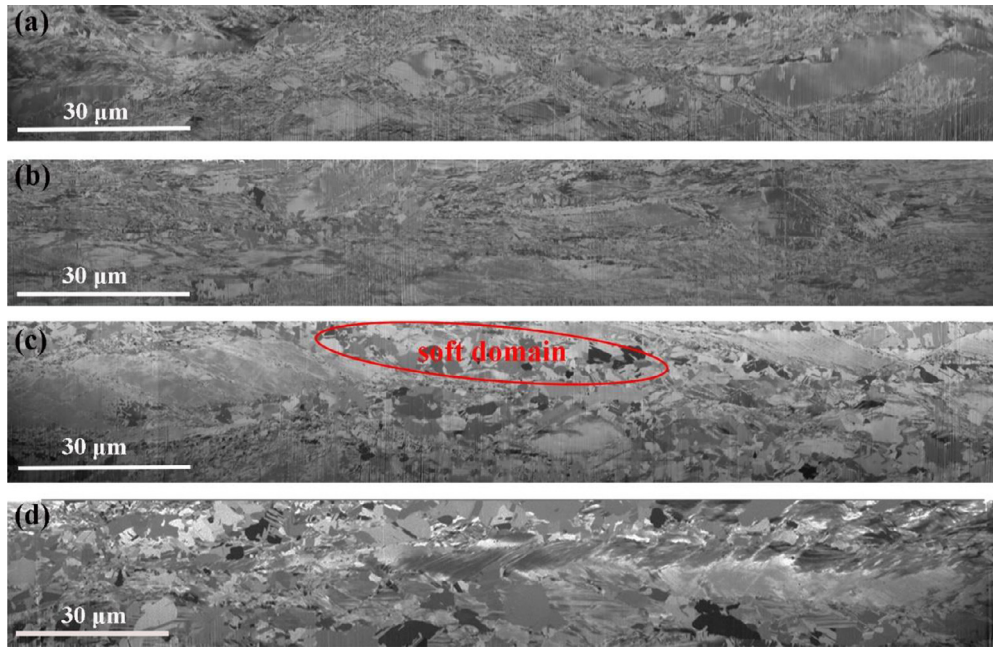


Fig. 2. Ion channeling image of typical microstructures in partially recrystallized brass: (a) R80; (b) R80+260C_10 min; (c) R80+260C_20 min (area 1 is a recrystallized soft domain lamellar); (d) R80+260C_30 min.

contain annealing twins, which are otherwise pristine in their interior with very low dislocation density.

3.2. Mechanical property

Uniaxial tensile tests were performed to measure the yield strength and ductility of the annealed brass, as shown in Fig. 4(a). The yield stress and uniform elongation of different samples are listed in Table 1. As shown in Fig. 4(c), the present HLS brass samples usually have combinations of stress and ductility superior to the published mechanical data with other microstructures [3,44–46]. Interestingly, contrast with the intuitive belief that increasing annealing time will increase ductility and decrease strength, the sample annealed at 260 °C for 20 min (R80+260C_20 min) retains the same yield strength as the sample annealed for 10 min (R80+260C_10 min) while acquiring a much higher ductility. As shown, R80+260C_20 min samples have the best combination of strength and ductility among these three HLS structures.

Fig. 4(b) shows that the R80+260C_20 min sample maintained a relatively high strain-hardening rate during the tensile deformation (even slightly higher than the R80+260C_30 min samples at strain <10%). High strain hardening is needed for high ductility [6,44] and good yield strength [20,45]. The high strain-hardening behavior of the R80+260C_20 min sample is likely caused by HDI hardening and the higher volume fraction of soft domains, compared with R80+260C_10 min. Based on previous reports [11,30,31], the volume fraction of domains, the distance between two soft domains and thickness of soft domains, are the three parameters believed to influence HDI hardening. The statistics of these parameters are shown in Table 2. The soft domains are carefully extracted from Fig. 2(a)–(d), which form a representative subset of the images. The volume fraction, thickness and inter-soft-domain distance are measured subsequently. The volume fraction is estimated by measuring the area fraction of the soft domains in the image [46,47]. These parameters are similar in the R80+260C_10 min and R80+260C_20 min samples. However, as shown in Fig. 4(a), the R80

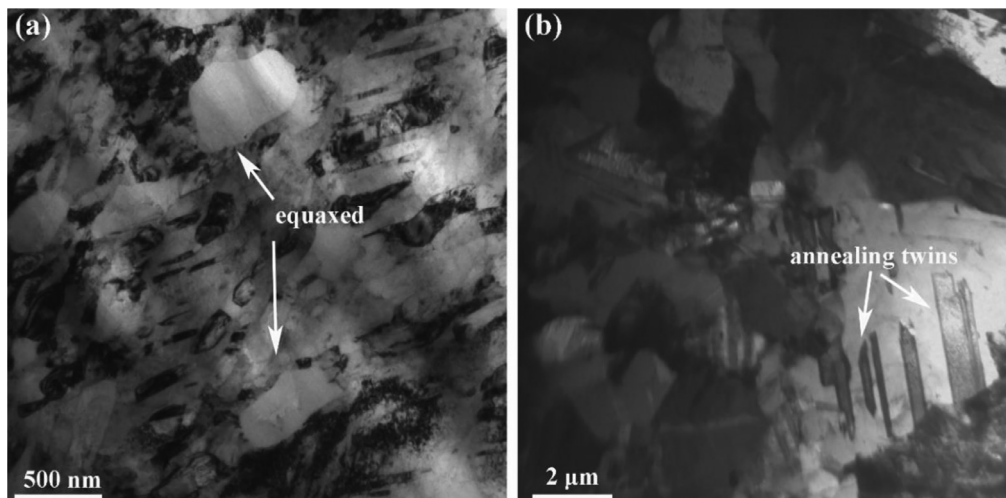


Fig. 3. TEM images of (a) a hard domain with ultrafine grains and (b) a soft domain with recrystallized coarse grains containing twins and very few dislocations.

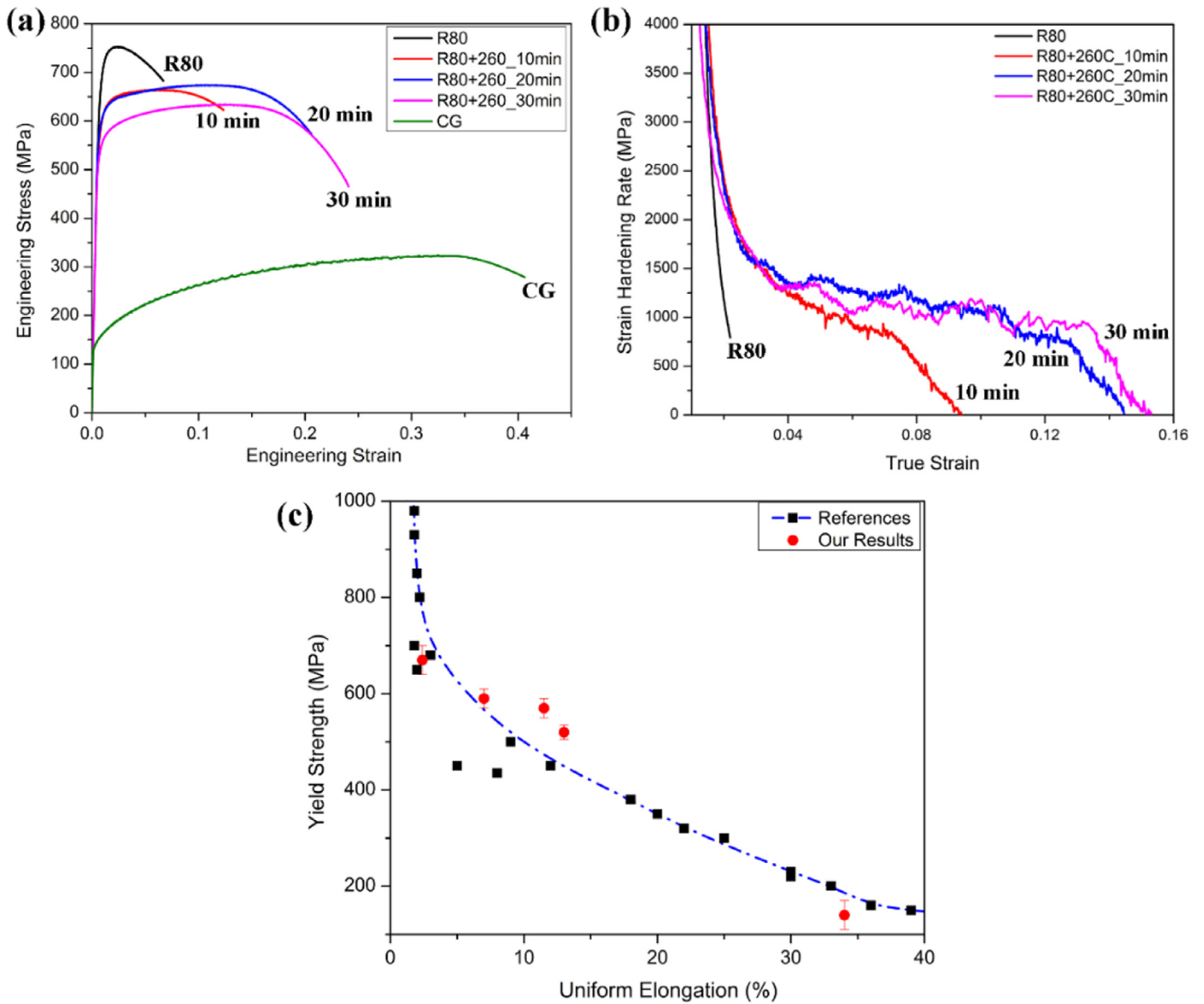


Fig. 4. (a) strain–stress curves of brass that was cold rolled for 80% thickness reduction and partially recrystallized at 260 °C for different periods; (b) strain-hardening rate curves for those samples shown in (a); (c) comparison of HLS and other structured brass [3,48–50].

Table 1
Mechanical properties of cold rolled and partially annealed brass.

	Yield stress (MPa)	Uniform elongation (%)
R80	680	2.5
R80+A260C_10 min	580	7
R80+A260C_20 min	570	12.5
R80+A260C_30 min	500	13.5
Coarse Grained (CG)	140	34

Table 2
Parameters for the heterogeneous structure.

	The volume fraction of soft domains (%)	The average distance between two soft domains (μm)	The average thickness of a soft domain (μm)
R80	15	~28	~8
R80+260C_10 min	30	~15	~13
R80+260C_20 min	45	~12	~15
R80+260C_30 min	70	<5	>20

+260C_20 min sample has 80% higher ductility, but the same yield strength as compared with the R80+260C_10 min sample. Meanwhile, a further increase of the volume fraction of soft domains, by annealing for a longer time of 30 mins, led to lower strength but the same ductility. Therefore, there should be additional unknown parameter(s) that impact(s) the HDI hardening of the HLS brass.

3.3. EBSD mapping and misorientation characterization

Electron backscattered diffraction (EBSD) was used to analyze a representative soft domain and its neighboring hard domains (Fig. 5). After annealing at 260 °C for 20 min, the fraction of low-angle grain boundaries ($< 15^\circ$) decreased by 50% as compared with the sample annealed for 10 min, and the distribution of grain boundary angles is similar to that of the sample annealed for 30 min. The result indicates that the partial recrystallization induces the emergence of the new high-angle boundaries across the soft/hard domain interfaces. After 30-min annealing, despite the high fraction of high-angle misorientation domain boundaries, it appears that the hard domains cannot provide enough constraint to soft domain due to their low volume fraction (Fig. 2(d)), which leads to a relatively low HDI stress, and low

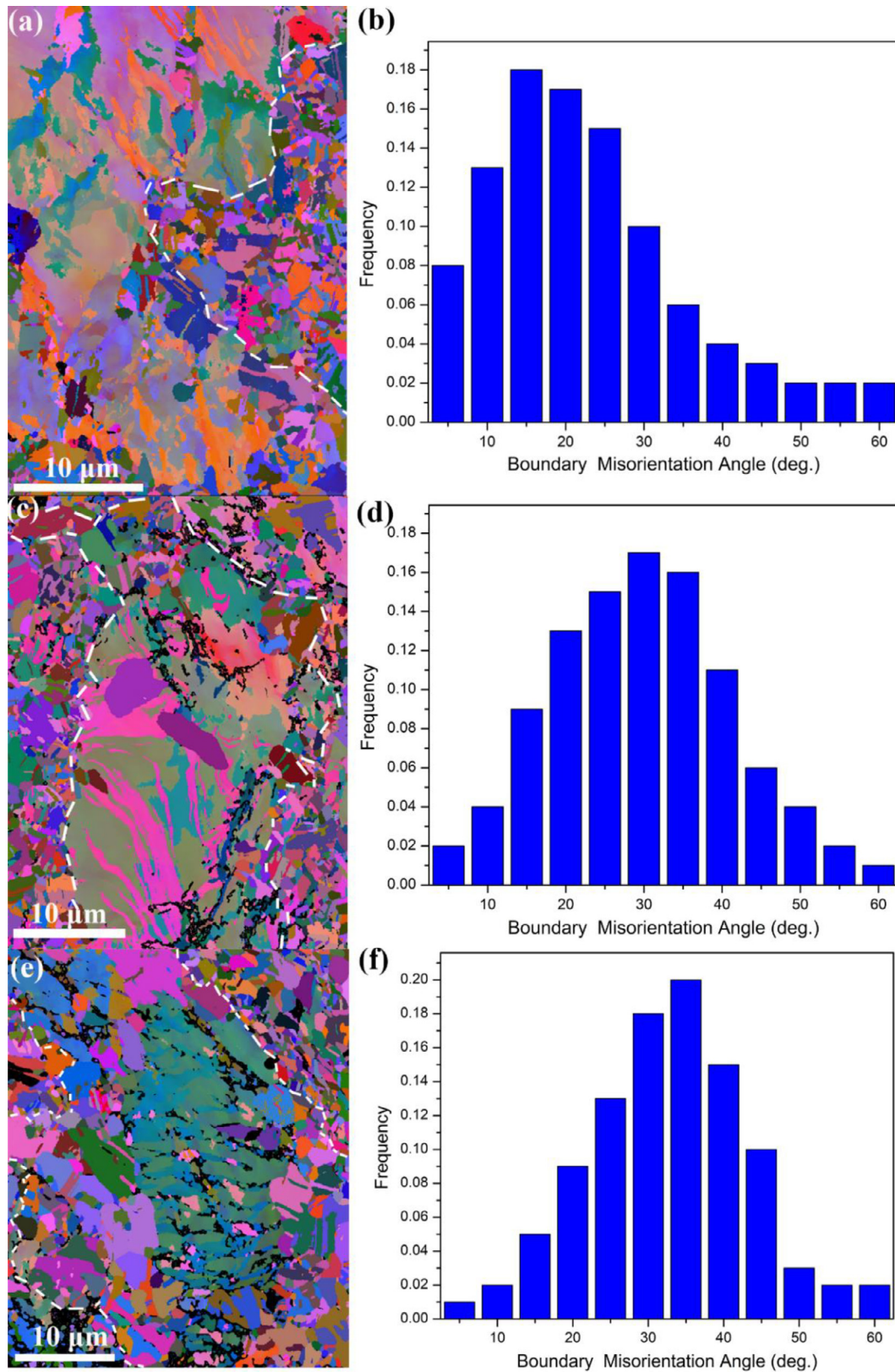


Fig. 5. EBSD data (all-Euler images) show representative regions where soft domains are embedded by hard domains. The right column shows the corresponding misorientation angle distribution along soft/hard domain boundaries: (a), (b) R80+260C_10 min; (c), (d) R80+260C_20 min; (e), (f) R80+260C_30 min.

yield strength of R80_260C_30 min. We define the domain misorientation as the average misorientation of the small grains (hard domains) and coarse grains (soft domain) at the interface (the white dotted line shows the interface for statistics).

The domain misorientations of R80_260C_10 min, R80_260C_20 min and R80_260C_30 min samples are 20°, 35° and 38°, respectively. A previous study revealed that a high volume fraction of high-angle grain boundaries could increase the ductility of metals by effectively blocking

dislocation slip in nanostructured and ultrafine-grained materials [51]. Fig. S2 shows that the distribution of misorientation in hard domains is similar for different annealing time. Thus, the improvement in ductility was not caused by the grain boundary misorientations in hard domains. These results indicate that high-angle domain boundaries have a significant impact on the ductility of the HLS brass. The main mechanism for the improvement of ductility is HDI hardening, which is caused by the evolution of GNDs. Moreover, domain misorientation significantly influences HDI stress evolution, which will be discussed later.

3.4. Dislocation analysis at different strain levels

Wu and Zhu [10,11] hypothesized that there exist three deformation stages for HLS materials: (1) In the elastic stage, both soft and hard domains deform elastically; (2) In the elastic-plastic stage, the hard domains deform elastically, while the soft domains deform plastically. Dislocations glide in the soft domains (coarse grains adjacent to domain boundaries) will be piled up at the domain boundaries, developing HDI stress; (3) In the plastic stage, both soft and hard domains deform plastically. Strain partitioning might occur with the soft domain carrying a higher fraction of plastic strain, which develops HDI hardening. This hypothesis needs to be further studied in HLS materials. More importantly, dislocation piling-ups at the domain boundaries, which is crucial for HDI stress evolution, should be examined. In the following, we focus on the deformation of R80+260C_20 min samples, which have the best combination of strength and ductility among the three HLS samples. Since the elastic stage is not important for dislocation interaction, we will skip this stage.

3.4.1. Elastic-plastic stage

An R80+260C_20 min sample was loaded in tension to 400 MPa, which was still in the overall elastic stage according to the stress-strain curve. However, X-ray diffraction (XRD) data in Fig. S3 show that the dislocation density in the sample has already increased. The further TEM analysis of the sample is shown in Fig. 6, which is inside a soft domain. Using two-beam condition [52] (Fig. 6(b) is the diffraction

pattern that guides the setup of two-beam condition imaging), the burgers vectors of arrow-marked dislocations were determined as $b_1 = \frac{a}{2} [1\bar{1}0]$ and $b_2 = \frac{a}{6} [\bar{1}12]$. Comparing the TEM micrographs in Fig. 6 (c)–(e) with that in Fig. 3(b) of a partially recrystallized sample, it can be concluded that these dislocations were formed during the tensile deformation. In other words, the soft domains deformed plastically during the apparently elastic stage. Moreover, Fig. 6(d) suggests that the dislocations were probably emitted from grain boundaries. Also, both partial and full lattice dislocations were active in the early deformation stage.

3.4.2. Low plastic deformation (<4.5% true strain)

Fig. 7(a) shows a coarse grain near a domain boundary (marked by the white dotted line) at the yield point. Two diffraction patterns are shown in Fig. 7(b) and (c), taken in the center of the grain and near the boundary, respectively, corresponding to the white circles. The diffraction at the domain boundary is highly distorted, which indicates that the area near the domain boundary has a higher strain, containing a higher density of dislocations. Meanwhile, an ultrafine grain with twins in a hard domain is shown in Fig. 7(d). Several partial dislocations were emitted from twin boundaries (Fig. 7(e)), which formed stacking faults (SFs) near the twin boundaries, indicating that small grains in the hard domains started plastic deformation.

With increasing plastic strain, the number of GND in the pile-ups and the pile-up length will increase. Fig. 8 shows a GND pile-up scenario at 3% plastic strain. The GND pile-ups vary with domain boundary angles. Table 3 is the analysis of 23 different domain boundaries with different domain boundary angles. As shown in Fig. 8, the number of piled-up dislocations per unit length (GND density in pile-ups) at high-angle boundaries ($>15^\circ$) is about 1.5 times of those at low-angle boundaries ($5^\circ - 15^\circ$). Meanwhile, the pile-up length is also longer at high-angle domain boundaries. The higher GND density in pile-ups and the longer pile-up length will generate higher HDI stresses [53]. In other words, high-angle domain boundaries produce high HDI hardening.

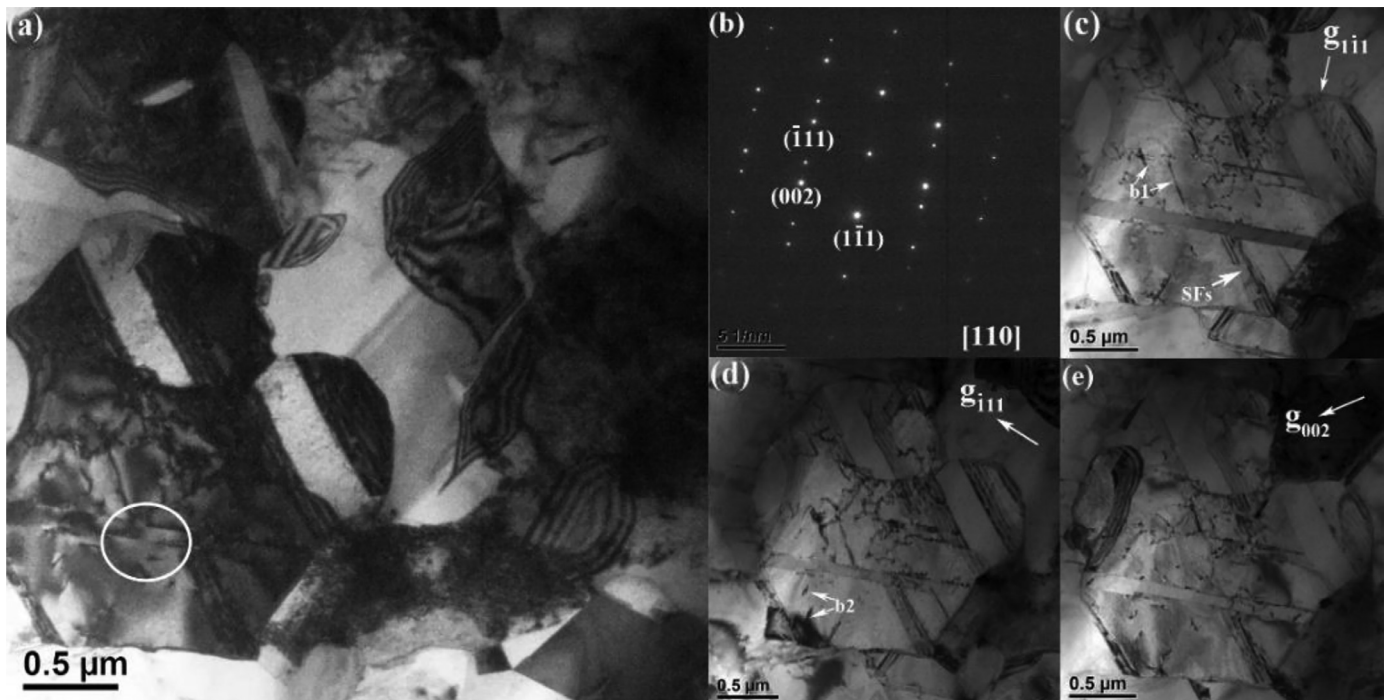


Fig. 6. (a) A TEM image of dislocations in a soft domain in the elastic deformation stage; (b) the diffraction corresponding to the circle in (a); (c)–(e) dislocations observed under different two-beam conditions.

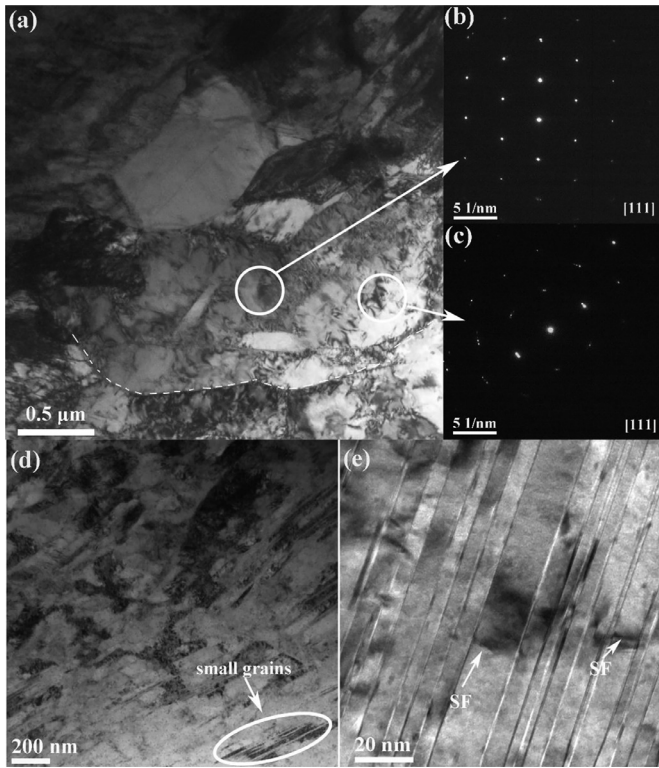


Fig. 7. TEM micrographs of brass at the yield point (a) a coarse grain at domain boundary; (b) and (c) two diffraction patterns from the inside of the grain (b) and near the boundary (c); (d) an ultrafine grain with twins in a hard domain; (e) high magnification of the ultrafine grains showing the SFs near twinning boundaries.

3.4.3. High plastic deformation

Fig. 9(a) shows a domain boundary at 9% plastic strain, as marked by the white dotted line. Fig. 9(b) and (c) shows that an ultrafine grain was heavily deformed, and twin boundaries became less coherent due to the plastic deformation. Partial dislocations were emitted not only from twin boundaries but also from grain boundaries. In the soft domains, a high density of dislocation walls and subgrains were formed, and the dislocation walls became a new source to impede dislocation movement, as shown in Fig. 9(e). Dislocation tangles were formed at domain boundaries, indicating that the domain boundaries began to lose the ability to support further GND pile-ups. Since the interaction of soft domains and hard domains was weakened at

high-strain levels, the HDI hardening might become weaker and dislocation density hardening probably dominates the strain hardening.

4. Discussion

4.1. Formation of HLS in brass

The most important factor for the formation of HLS brass is the heterogeneity of deformation during cold rolling [54,55], which elongated the initial coarse grains and produced a high density of dislocation cells and subgrains [56]. Some of these substructures were further deformed into ultrafine grains with twins [57]. The dislocation cells and elongated ultrafine grains after rolling are shown in Fig. S1. The soft domains in HLS are from the new recrystallized grains with early nucleation and high growth rate.

The hard domains are composed of two different types of grains: elongated ultrafine grains and new recrystallized ultrafine grains. As shown in Fig. 3(a), some of the elongated grains formed during rolling were not recrystallized during annealing and maintained sharp boundaries. The other type was formed by “clustering” of the newly recrystallized but small grains. During the annealing, dislocation cells might act as potential heterogeneous nucleation sites for recrystallization. Due to the variation in the initial cell sizes and cell boundary misorientations, the mobility of the boundaries of the newly recrystallized grains is different [58,59]. Recrystallized grains having a lower growth rate ended up with their size still less than 1 μm after annealing and became part of the hard domains.

The HLS brass in this study is different from the HLS Ti reported earlier [11]. First, the texture change and average misorientation is usually small during partial annealing of Ti after rolling [60,61], and the texture is known to influence the mechanical property of hcp metals and alloys significantly. However, in isotropic fcc materials such as brass, the recrystallization often changes the texture by producing new grains with high-angle grain boundaries [62,63]. Second, most grains remained elongated in the hard domains of Ti [11], while most grains of hard domains in brass here are equiaxed, shown in Figs. 3(a) and 5, implying that different grain shapes might be needed to obtain the best combination of strength and ductility in anisotropic and isotropic materials, respectively [64].

4.2. Strain hardening mechanism

For conventional homogeneous materials, dislocation strengthening, also known as Taylor hardening, is the primary hardening mechanism while straining [43]. However, in heterostructured materials,

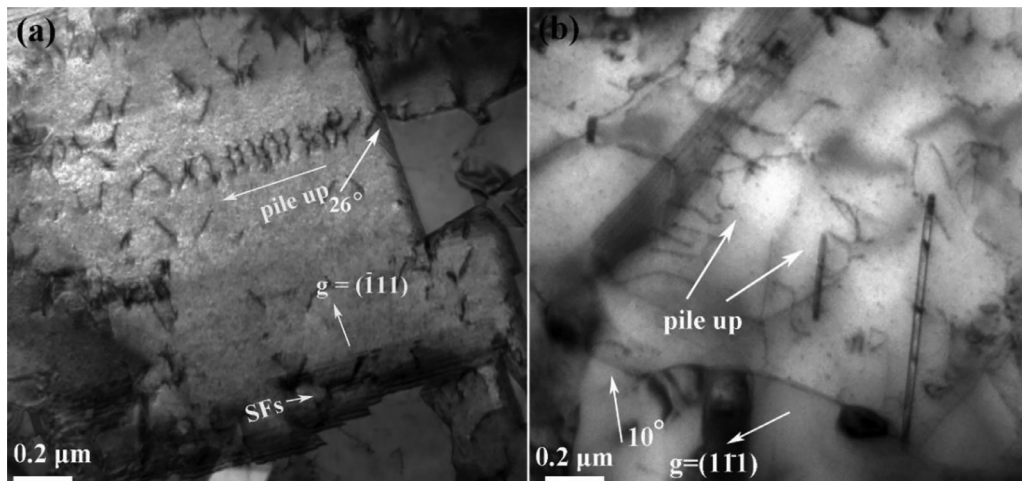


Fig. 8. TEM images of GND pile-ups at 3% plastic strain at (a) a high-angle domain boundary ($>15^\circ$); (b) a low-angle domain boundary (5° – 15°).

Table 3
GND pile-up analysis at domain boundaries.

	Number of domains	Average misorientation (°)	Average pile-up length (μm)	Average number of pile-up	Number of piled-up dislocations per unit length (μm ⁻¹)	Average inter-pile-up spacing (μm)
Low angle domains	11	~13	~0.8	10	12.5	~0.071
High angle domains	12	~28	~1.1	19	17.3	~0.039

it has been reported that HDI hardening is rather prominent and even higher than Taylor hardening [10,14]. Both of them, though, are associated with GND pile-ups to different extents. A critical issue is to evaluate and compare their respective roles in the work hardening process of HLS materials at various applied strains. In this section, we will discuss the respective evolution of each hardening process and identify their contributions at different straining stages.

4.2.1. Dislocation strengthening

Dislocation strengthening can be described by Taylor's equation [38,65,66]:

$$\sigma_{dislocation} = M\alpha Gb\sqrt{\rho} \quad (1)$$

where M is the Taylor factor, G is the shear elastic modulus, b is the magnitude of the Burger's vector, ρ is dislocation density, and α is a coefficient often taken to be 0.2–0.7. Also, the strain hardening caused by dislocation accumulation can be described as [67]:

$$\frac{d\sigma_{dislocation}}{d\varepsilon} = M\alpha Gb \frac{d\sqrt{\rho}}{d\varepsilon} = M\alpha Gb \frac{d\sqrt{\rho_s + \rho_G}}{d\varepsilon} \quad (2)$$

where ε is the applied strain, ρ_s is the density of statistically stored dislocations (SSDs), and ρ_G is the GND density.

Fig. 10(a) shows the total dislocation density evolution in the R80_A260C_10 min, R80_A260C_20 min and R80_A260C_30 min samples at different strain levels. The dislocation density of different samples was calculated from XRD data, as shown in Fig. S4. The dislocation density in the R80_A260C_10 min sample is almost twice of that in the R80_A260C_20 min sample at low plastic strains (less than 4.5%), but their yield strengths are similar, as shown in Fig. 4(a). Meanwhile, the dislocation hardening rate in the different samples is shown in Fig. 10(b). The dislocation hardening rate in the R80_A260C_30 min sample is significantly higher than that in the R80_A260C_20 min sample at early plastic deformation, but the total strain hardening rate, as shown in Fig. 4(b), is slightly lower than in the R80_A260C_20 min sample. Therefore, dislocation hardening itself is not the dominant work hardening mechanism at the early plastic deformation stage of the HLS brass, and another hardening process is expected to play a crucial role at the early plastic deformation stage. As discussed later, this mechanism is HDI hardening. Additionally, the inconsistency between the dislocation hardening rate and total strain hardening rate at early plastic deformation also indicates the inability of the simple ρ_G term in the Taylor equation to capture the effect of GNDs at domain boundaries. Whereas at the later straining stage, the predicted order of dislocation-hardening

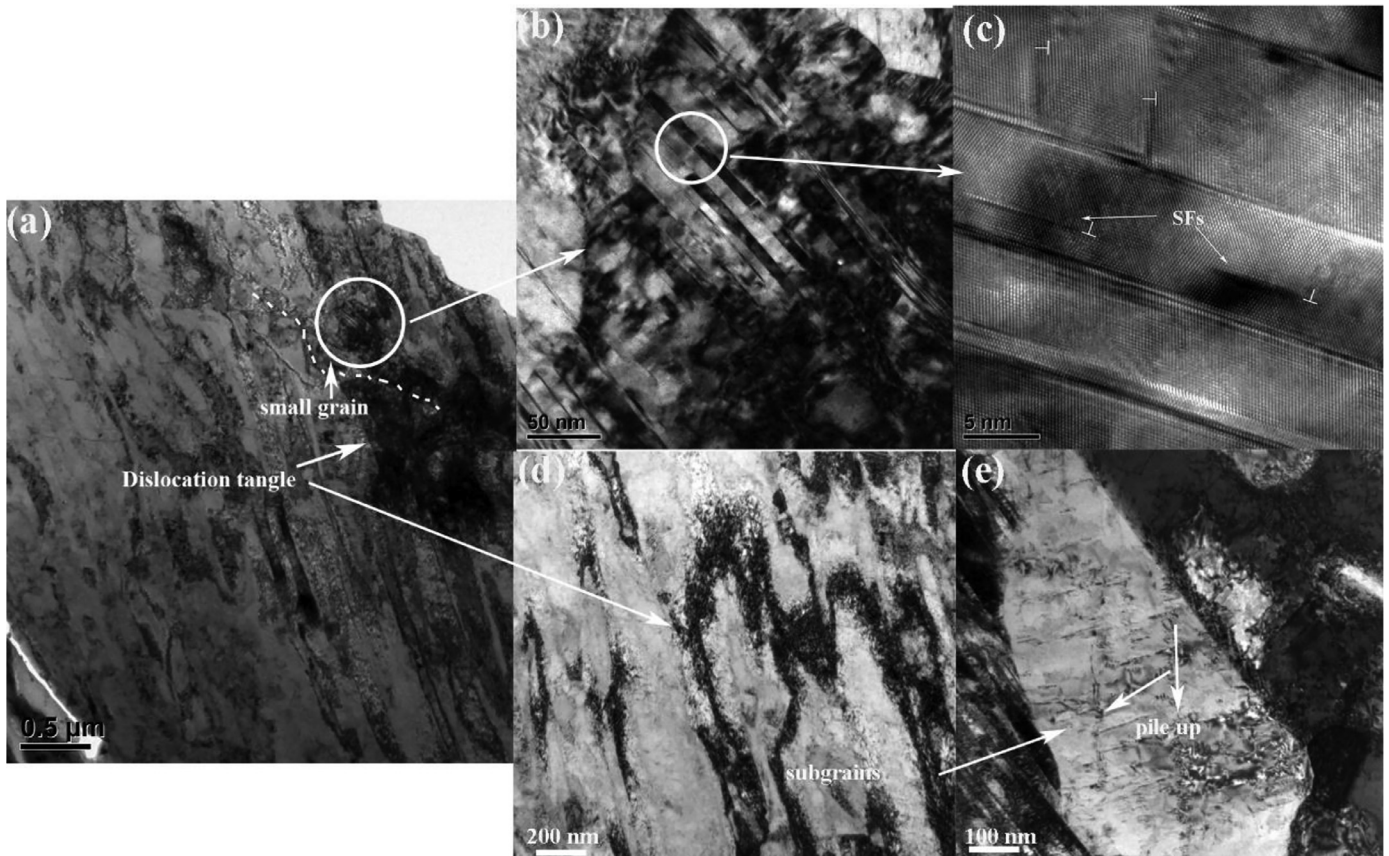


Fig. 9. (a) a domain boundary with a high density of dislocation; (b)–(c) an ultrafine grain containing a high density of twins in the hard domain and dislocations evolution in the grain; (d)–(e) newly formed dislocation cells in the soft domain.

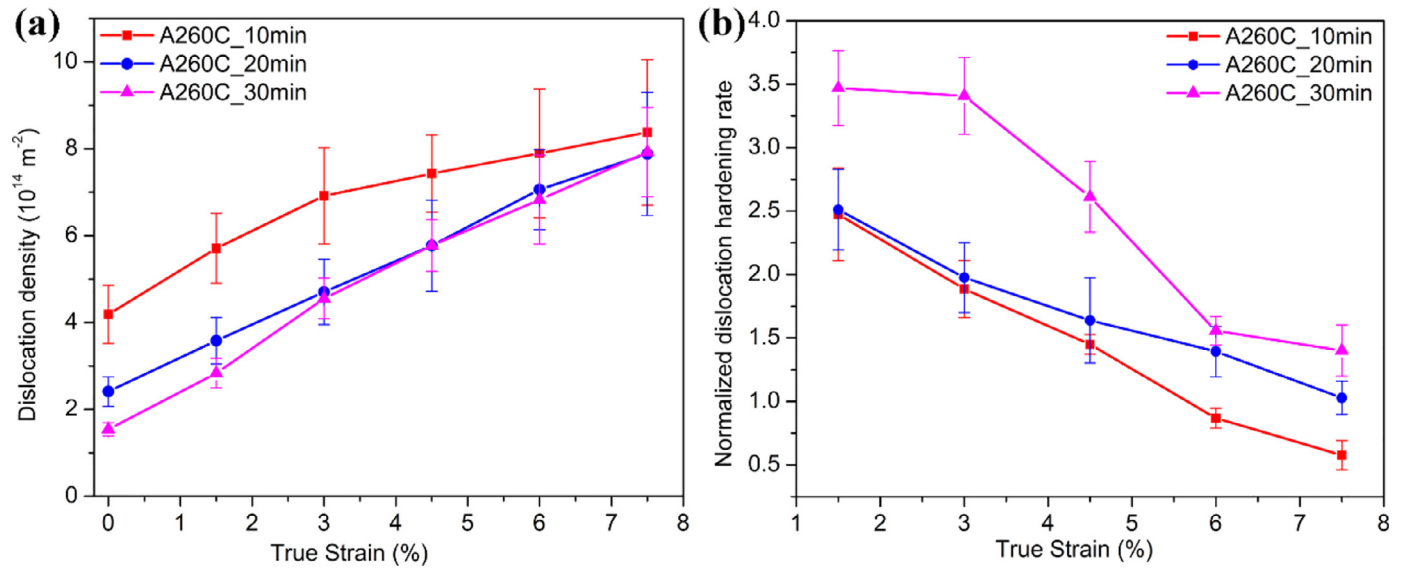


Fig. 10. (a) dislocation density evolution at different strain levels of samples annealed for different time; (b) normalized dislocation hardening rate ($\Delta\rho^{1/2}/\Delta\varepsilon$)/(MaGb) at different strain levels for samples annealed for different time.

effectiveness in three samples agrees well with the measured overall working hardening rate in Fig. 4(b). Thus, dislocation hardening is predominant at high plastic deformation stage.

4.2.2. HDI hardening

Fig. 11 shows the HDI stress of different partially recrystallized samples. HDI stress was measured by using the loading-unloading-reloading (LUR) test [10,11,68], and the sample geometry is the same as in the uniaxial tensile test. The method to calculate HDI stress was proposed by Yang et al. [68]:

$$\sigma_{HDI} = \frac{\sigma_r + \sigma_u}{2} \quad (3)$$

where σ_{HDI} is the HDI stress, σ_r is the reloading yield stress, σ_u is the unloading yield stress. In our calculation, unloading yield stress is defined as the point where elastic modulus reduction is 10% in unloading state [68].

The R80_A260C_20 min sample has the highest HDI stress, which is the reason for its high yield stress. Meanwhile, HDI hardening became a substantial part of the total strain hardening, which

influences the ductility. The HDI hardening is defined as,

$$\Theta_{HDI} = \frac{d\sigma_{HDI}}{d\varepsilon} \quad (4)$$

where Θ_{HDI} is the slope in Fig. 11(b), σ_{HDI} is the HDI stress. At a relatively low strain level (less than 7% in Fig. 11(b)), the HDI hardening dominated the total strain hardening. Specifically, the HDI hardening is ~ 1 GPa between 2% and 7%, which is the main component for the total strain hardening. In comparison, due to the low HDI hardening in the R80+A260C_10 min sample, the ductility of the sample is significantly lower than R80+A260C_20 min and R80+A260C_30 min samples.

Fig. 11 shows that the HDI stress initially increased with applied strain almost linearly for strains far beyond yielding, indicating the continuous accumulation of GNDs near the domain boundaries during the plastic deformation. The HDI hardening can be regarded as the slope of the curve in Fig. 11(b). As shown, the HDI hardening is more significant at low plastic strains and the R80+A260C_20 min sample has the highest value among the three, coinciding with the overall working hardening behavior and confirming the dominating

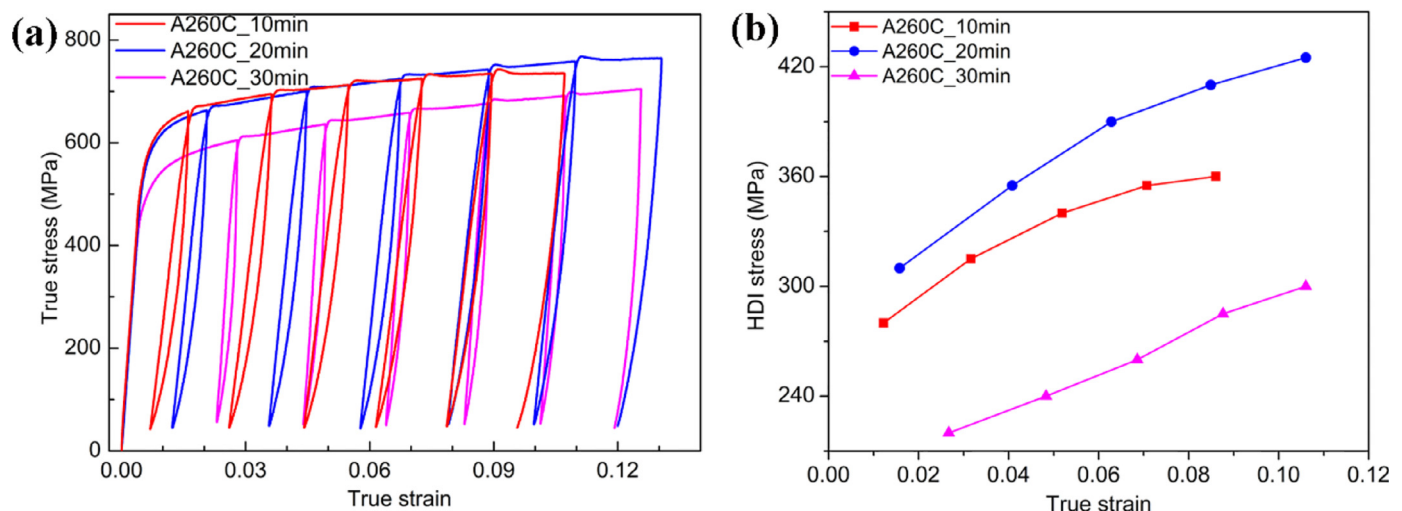


Fig. 11. (a) Loading-unloading-reloading (LUR) test to measure the HDI stress; (b) HDI stress calculated from the LUR curves.

role of HDI hardening in early deformation stage. The HDI hardening becomes weaker at large applied strains, possibly because the interactions of the GNDs with gliding dislocations make it more difficult to accumulate GNDs effectively at domain boundaries. At high flow stresses, it is also possible for the dislocations to be pushed into the domain boundaries, or to cross slip if the stacking fault energy (SFE) is not too low [34]. SFE is expected to have a significant effect on the GND piling-up, and consequently on the HDI hardening. For example, Fig. 8 shows well developed GND pile-ups in the low SFE brass. However, this was not observed in the in-situ observation during the deformation of copper [34], in which Frank–Read dislocation sources were found to be dynamically activated and deactivated. GND pile-ups often disappear when a Frank–Read source was deactivated. The different dislocation activity between copper and brass is probably because copper has a much higher SFE than brass, making it easier for dislocations to cross-slip. This issue needs to be further studied.

4.3. Domain misorientation influence on HDI hardening

It has been reported [30,31,69,70] that the domain thickness and inter-domain spacing are critical factors to influence HDI hardening. There exists an optimum spacing that corresponds to the maximum distance for GNDs pile-up [30,31]. Although the R80+A260C_10 min and R80+A260C_20 min samples have similar average thickness and inter-distance of soft domains, as shown in Table 1, the uniform elongation of the R80+A260C_20 min sample is ~80% higher than that of the R80+A260C_10 min sample, while the yield strength for these two samples is almost the same. Thus, there should be other source(s) to influence the HDI hardening in the present scenario. The microstructural parameter with the most dramatic difference in these two samples is domain boundary misorientation, as shown in Fig. 5, which is potentially another crucial parameter that influences HDI hardening.

The role of domain boundary misorientation on HDI hardening has been not well studied so far. Wu et al. [11] reported extraordinary HDI hardening in Ti fabricated by asymmetric rolling and partial recrystallization. Variation of misorientation across domain boundary was not considered, because it changes little (usually less than 5°) in the partially annealed Ti [60]. Ma et al. and Huang et al. utilized laminated materials to study the influence of domain interface on HDI stress [30,31]. However, the effect of misorientation was not among the factors studied. In our HLS brass, the most significant difference between R80+A260C_20 min and R80+A260C_10 min samples is the misorientation across domain boundaries, whose averages are 35° and 20°, respectively. As provided in Table 3, the average GND density in pile-ups and the pile-up length are significantly larger at the high-angle domain boundaries than those at low-angle counterparts. As discussed earlier, higher GND pile-up density and longer pile-up length are expected to produce higher HDI stress [34,53], which consequently produces higher HDI hardening, as verified in Fig. 11(b). Meanwhile, high-angle domain boundaries are capable of storing more dislocations [71], which could provide more space for GND pile-ups. Another reason for high domain misorientation to generate high HDI stress is the difficulty for slip transfer [72]. Thus, more dislocation pile-ups are needed to accumulate stress and activate slip systems across the domain boundary. As such, the HDI hardening at the presence of high-angle domain boundaries becomes much more significant.

5. Conclusion

Heterogeneous lamellar structure (HLS) brass samples, with a superior combination of strength and ductility, were fabricated by rolling and partial recrystallization. The volume fraction of soft domains, the thickness/spacing of soft domains and the misorientation of domains were found to affect HDI hardening. The strain

hardening behavior and mechanisms at different plastic deformation stages were investigated. The main conclusions are summarized below:

1. There exists an optimum HLS structure for the best combination of strength and ductility. This optimum structure for HLS brass was produced by rolling and partial recrystallization in the R80_260C_20 min sample.
2. The HLS brass has three deformation stages: (1) coarse grains firstly deform at elastic stage; (2) dislocation pile-ups are formed due to the plastic strain gradient at the domain boundaries, and the pile-up length and inter-spacing increase with the applied plastic strain; (3) at high plastic strain, dislocation entanglement is formed at the domain boundary, and new cell boundaries become new sites for dislocation pile-ups.
3. At the early plastic deformation stage (true strain <4.5%), HDI hardening was the primary hardening mechanism for HLS brass, which corresponds to the GND pile-ups at domain boundaries. At high strain level (true strain level higher than 7%), dislocation hardening becomes more important, and a high density of dislocation cells was formed inside soft domains, which indicates that the interaction between soft and hard domains becomes weaker.
4. Besides the volume fraction and the thickness/spacing of soft domains, domain misorientation is suggested to be another crucial heterostructural parameter that significantly influences HDI hardening.

Declaration of Competing Interest

The authors declare that they have no known competing financial interests or personal relationships that could have appeared to influence the work reported in this paper.

Acknowledgements

This project was supported by the US Army Research Office [W911 NF-12-1-0009]. EBSD, TEM and XRD characterization were performed in part at the AIF facility which is supported by the State of North Carolina and the National Science Foundation [ECCS-1542015]. The AIF is a member of the North Carolina Research Triangle Nanotechnology Network (RTNN), a site in the National Nanotechnology Coordinated Infrastructure (NNCI).

Supplementary materials

Supplementary material associated with this article can be found in the online version at doi:[10.1016/j.actamat.2020.01.037](https://doi.org/10.1016/j.actamat.2020.01.037).

References

- [1] Y. Zhao, T. Topping, J.F. Bingert, J.J. Thornton, A.M. Dangelewicz, Y. Li, W. Liu, Y. Zhu, Y. Zhou, E.J. Lavernia, High tensile ductility and strength in bulk nanostructured nickel, *Adv. Mater.* 20 (2008) 3028–3033, doi: [10.1002/adma.200800214](https://doi.org/10.1002/adma.200800214).
- [2] Y.H. Zhao, X.Z. Liao, S. Cheng, E. Ma, Y.T. Zhu, Simultaneously increasing the ductility and strength of nanostructured alloys, *Adv. Mater.* 18 (2006) 2280–2283, doi: [10.1002/adma.200600310](https://doi.org/10.1002/adma.200600310).
- [3] H. Bahmanpour, K.M. Youssef, J. Horky, D. Setman, M.A. Atwater, M.J. Zehetbauer, R.O. Scattergood, C.C. Koch, Deformation twins and related softening behavior in nanocrystalline Cu–30% Zn alloy, *Acta Mater.* 60 (2012) 3340–3349, doi: [10.1016/j.actamat.2012.02.036](https://doi.org/10.1016/j.actamat.2012.02.036).
- [4] K. Youssef, M. Sakaliyska, H. Bahmanpour, R. Scattergood, C. Koch, Effect of stacking fault energy on mechanical behavior of bulk nanocrystalline Cu and Cu alloys, *Acta Mater.* 59 (2011) 5758–5764, doi: [10.1016/j.actamat.2011.05.052](https://doi.org/10.1016/j.actamat.2011.05.052).
- [5] C.X. Huang, W.P. Hu, Q.Y. Wang, C. Wang, G. Yang, Y.T. Zhu, An ideal ultrafine-grained structure for high strength and high ductility, *Mater. Res. Lett.* 3 (2015) 88–94, doi: [10.1080/21663831.2014.968680](https://doi.org/10.1080/21663831.2014.968680).
- [6] I.A. Ovid'ko, R.Z. Valiev, Y.T. Zhu, Review on superior strength and enhanced ductility of metallic nanomaterials, *Prog. Mater. Sci.* 94 (2018) 462–540, doi: [10.1016/j.pmatsci.2018.02.002](https://doi.org/10.1016/j.pmatsci.2018.02.002).

- [7] R.Z. Valiev, Y. Estrin, Z. Horita, T.G. Langdon, M.J. Zehetbauer, Y.T. Zhu, Fundamentals of superior properties in bulk nanoscale materials, *Mater. Res. Lett.* 4 (2016) 1–21, doi: [10.1080/21663831.2015.1060543](https://doi.org/10.1080/21663831.2015.1060543).
- [8] B.B. He, B. Hu, H.W. Yen, G.J. Cheng, Z.K. Wang, H.W. Luo, M.X. Huang, High dislocation density-induced large ductility in deformed and partitioned steels, *Science* 357 (2017) 1029–1032, doi: [10.1126/science.aan0177](https://doi.org/10.1126/science.aan0177).
- [9] Y.T. Zhu, X.L. Wu, Ductility and plasticity of nanostructured metals: differences and issues, *Mater. Today Nano* 2 (2018) 15–20, doi: [10.1016/j.mtnano.2018.09.004](https://doi.org/10.1016/j.mtnano.2018.09.004).
- [10] X. Wu, Y. Zhu, Heterogeneous materials: a new class of materials with unprecedented mechanical properties, *Mater. Res. Lett.* 5 (2017) 527–532, doi: [10.1080/21663831.2017.1343208](https://doi.org/10.1080/21663831.2017.1343208).
- [11] X. Wu, M. Yang, F. Yuan, G. Wu, Y. Wei, X. Huang, Y. Zhu, Heterogeneous lamella structure unites ultrafine-grain strength with coarse-grain ductility, *Proc. Natl. Acad. Sci.* 112 (2015) 14501–14505, doi: [10.1073/pnas.1517193112](https://doi.org/10.1073/pnas.1517193112).
- [12] X.L. Wu, P. Jiang, L. Chen, J.F. Zhang, F.P. Yuan, Y.T. Zhu, Synergetic strengthening by gradient structure, *Mater. Res. Lett.* 2 (2014) 185–191, doi: [10.1080/21663831.2014.935821](https://doi.org/10.1080/21663831.2014.935821).
- [13] X. Wu, Y. Zhu, Heterogeneous materials: a new class of materials with unprecedented mechanical properties, *Mater. Res. Lett.* 5 (2017) 527–532, doi: [10.1080/21663831.2017.1343208](https://doi.org/10.1080/21663831.2017.1343208).
- [14] Y. Zhu, X. Wu, Perspective on hetero-deformation induced (HDI) hardening and back stress, *Mater. Res. Lett.* 7 (2019) 393–398, doi: [10.1080/21663831.2019.1616331](https://doi.org/10.1080/21663831.2019.1616331).
- [15] Y. Wang, M. Chen, F. Zhou, E. Ma, High tensile ductility in a nanostructured metal, *Nature* 419 (2002) 912–915, doi: [10.1038/nature01133](https://doi.org/10.1038/nature01133).
- [16] B.O. Han, E.J. Lavernia, Z. Lee, S. Nutt, D. Witkin, Deformation behavior of bimodal nanostructured 5083 Al alloys, *Metall. Mater. Trans. A* 36 (2005) 957–965, doi: [10.1007/s11661-005-0289-7](https://doi.org/10.1007/s11661-005-0289-7).
- [17] R.Q. Ye, B.Q. Han, E.J. Lavernia, Simulation of deformation and failure process in bimodal Al alloys, *Metall. Mater. Trans. A* 36 (2005) 1833–1840, doi: [10.1007/s11661-005-0047-x](https://doi.org/10.1007/s11661-005-0047-x).
- [18] T.H. Fang, W.L. Li, N.R. Tao, K. Lu, Revealing extraordinary intrinsic tensile plasticity in gradient nano-grained copper, *Science* 331 (2011) 1587–1590, doi: [10.1126/science.1200177](https://doi.org/10.1126/science.1200177).
- [19] H.W. Huang, Z.B. Wang, J. Lu, K. Lu, Fatigue behaviors of AISI 316L stainless steel with a gradient nanostructured surface layer, *Acta Mater.* 87 (2015) 150–160, doi: [10.1016/j.actamat.2014.12.057](https://doi.org/10.1016/j.actamat.2014.12.057).
- [20] X. Wu, P. Jiang, L. Chen, F. Yuan, Y.T. Zhu, Extraordinary strain hardening by gradient structure, *Proc. Natl. Acad. Sci.* 111 (2014) 7197–7201, doi: [10.1073/pnas.1324069111](https://doi.org/10.1073/pnas.1324069111).
- [21] Z. Cheng, H. Zhou, Q. Lu, H. Gao, L. Lu, Extra strengthening and work hardening in gradient nanotwinned metals, *Science* 362 (2018) eaa1925, doi: [10.1126/science.aau1925](https://doi.org/10.1126/science.aau1925).
- [22] J. Li, Y. Cao, B. Gao, Y. Li, Y. Zhu, Superior strength and ductility of 316L stainless steel with heterogeneous lamella structure, *J. Mater. Sci.* 53 (2018) 10442–10456, doi: [10.1007/s10853-018-2322-4](https://doi.org/10.1007/s10853-018-2322-4).
- [23] X. Fang, G. He, M. Ruiz, C. Zheng, Y. Wang, Z. Li, Y. Zhu, Influence of annealing parameters on the mechanical properties of heterogeneous lamella structured 5083 aluminum alloy, *Lett. Mater.* 9 (2019) 556–560, doi: [10.22226/2410-3535-2019-4-556-560](https://doi.org/10.22226/2410-3535-2019-4-556-560).
- [24] Z. Zhang, S.K. Vajpai, D. Orlov, K. Ameyama, Improvement of mechanical properties in SUS304L steel through the control of bimodal microstructure characteristics, *Mater. Sci. Eng. A* 598 (2014) 106–113, doi: [10.1016/j.msea.2014.01.023](https://doi.org/10.1016/j.msea.2014.01.023).
- [25] S.K. Vajpai, M. Ota, T. Watanabe, R. Maeda, T. Sekiguchi, T. Kusaka, K. Ameyama, The development of high performance Ti-6Al-4V Alloy via a unique microstructural design with bimodal grain size distribution, *Metall. Mater. Trans. A* 46 (2015) 903–914, doi: [10.1007/s11661-014-2649-7](https://doi.org/10.1007/s11661-014-2649-7).
- [26] C. Sawangrat, S. Kato, D. Orlov, K. Ameyama, Harmonic-structured copper: performance and proof of fabrication concept based on severe plastic deformation of powders, *J. Mater. Sci.* 49 (2014) 6579–6585, doi: [10.1007/s10853-014-8258-4](https://doi.org/10.1007/s10853-014-8258-4).
- [27] K. Park, M. Nishiyama, N. Nakada, T. Tsuchiyama, S. Takaki, Effect of the martensite distribution on the strain hardening and ductile fracture behaviors in dual-phase steel, *Mater. Sci. Eng. A* 604 (2014) 135–141, doi: [10.1016/j.msea.2014.02.058](https://doi.org/10.1016/j.msea.2014.02.058).
- [28] M. Calcagnotto, Y. Adachi, D. Ponge, D. Raabe, Deformation and fracture mechanisms in fine- and ultrafine-grained ferrite/martensite dual-phase steels and the effect of aging, *Acta Mater.* 59 (2011) 658–670, doi: [10.1016/j.actamat.2010.10.002](https://doi.org/10.1016/j.actamat.2010.10.002).
- [29] Z. Li, K.G. Pradeep, Y. Deng, D. Raabe, C.C. Tasan, Metastable high-entropy dual-phase alloys overcome the strength–ductility trade-off, *Nature* 534 (2016) 227–230, doi: [10.1038/nature17981](https://doi.org/10.1038/nature17981).
- [30] X. Ma, C. Huang, J. Moering, M. Ruppert, H.W. Höppel, M. Göken, J. Narayan, Y. Zhu, Mechanical properties of copper/bronze laminates: role of interfaces, *Acta Mater.* 116 (2016) 43–52, doi: [10.1016/j.actamat.2016.06.023](https://doi.org/10.1016/j.actamat.2016.06.023).
- [31] C.X. Huang, Y.F. Wang, X.L. Ma, S. Yin, H.W. Höppel, M. Göken, X.L. Wu, H.J. Gao, Y.T. Zhu, Interface affected zone for optimal strength and ductility in heterogeneous laminate, *Mater. Today* (2018), doi: [10.1016/j.mattod.2018.03.006](https://doi.org/10.1016/j.mattod.2018.03.006).
- [32] I.J. Beyerlein, J.R. Mayeur, S. Zheng, N.A. Mara, J. Wang, A. Misra, Emergence of stable interfaces under extreme plastic deformation, *Proc. Natl. Acad. Sci.* 111 (2014) 4386–4390, doi: [10.1073/pnas.1319436111](https://doi.org/10.1073/pnas.1319436111).
- [33] H. Gao, Mechanism-based strain gradient plasticity? I. theory, *J. Mech. Phys. Solids* 47 (1999) 1239–1263, doi: [10.1016/S0022-5096\(98\)00103-3](https://doi.org/10.1016/S0022-5096(98)00103-3).
- [34] H. Zhou, C. Huang, X. Sha, L. Xiao, X. Ma, H.W. Höppel, M. Göken, X. Wu, K. Ameyama, X. Han, Y. Zhu, *In-situ* observation of dislocation dynamics near heterostructured interfaces, *Mater. Res. Lett.* 7 (2019) 376–382, doi: [10.1080/21663831.2019.1616330](https://doi.org/10.1080/21663831.2019.1616330).
- [35] I. Brough, P.S. Bate, F.J. Humphreys, Optimising the angular resolution of EBSD, *Mater. Sci. Technol.* 22 (2006) 1279–1286, doi: [10.1179/174328406X130902](https://doi.org/10.1179/174328406X130902).
- [36] J. Jiang, T.B. Britton, A.J. Wilkinson, Measurement of geometrically necessary dislocation density with high resolution electron backscatter diffraction: effects of detector binning and step size, *Ultramicroscopy* 125 (2013) 1–9, doi: [10.1016/j.ultramic.2012.11.003](https://doi.org/10.1016/j.ultramic.2012.11.003).
- [37] Y.H. Zhao, X.Z. Liao, Z. Jin, R.Z. Valiev, Y.T. Zhu, Microstructures and mechanical properties of ultrafine grained 7075 Al alloy processed by ECAP and their evolutions during annealing, *Acta Mater.* 52 (2004) 4589–4599, doi: [10.1016/j.actamat.2004.06.017](https://doi.org/10.1016/j.actamat.2004.06.017).
- [38] T. Koizumi, M. Kuroda, Grain size effects in aluminum processed by severe plastic deformation, *Mater. Sci. Eng. A* 710 (2018) 300–308, doi: [10.1016/j.msea.2017.10.077](https://doi.org/10.1016/j.msea.2017.10.077).
- [39] N. Hansen, X. Huang, D.A. Hughes, Microstructural evolution and hardening parameters, *Mater. Sci. Eng. A* 317 (2001) 3–11, doi: [10.1016/S0921-5093\(01\)01191-1](https://doi.org/10.1016/S0921-5093(01)01191-1).
- [40] R. Ueji, N. Tsuji, Y. Minamino, Y. Koizumi, Ultragrain refinement of plain low carbon steel by cold-rolling and annealing of martensite, *Acta Mater.* 50 (2002) 4177–4189.
- [41] J.E. Burke, D. Turnbull, Recrystallization and grain growth, *Prog. Met. Phys.* 3 (1952) 220–292.
- [42] X. Huang, N. Hansen, N. Tsuji, Hardening by annealing and softening by deformation in nanostructured metals, *Science* 312 (2006) 249–251.
- [43] K. Marthinsen, O. Lohne, E. Nes, The development of recrystallization microstructures studied experimentally and by computer simulation, *Acta Metall.* 37 (1989) 135–145, doi: [10.1016/0001-6160\(89\)90273-3](https://doi.org/10.1016/0001-6160(89)90273-3).
- [44] Y.T. Zhu, X.Z. Liao, X.L. Wu, Deformation twinning in nanocrystalline materials, *Prog. Mater. Sci.* 57 (2012) 1–62, doi: [10.1016/j.pmatsci.2011.05.001](https://doi.org/10.1016/j.pmatsci.2011.05.001).
- [45] X.L. Ma, C.X. Huang, W.Z. Xu, H. Zhou, X.L. Wu, Y.T. Zhu, Strain hardening and ductility in a coarse-grain/nanostructure laminate material, *Scr. Mater.* 103 (2015) 57–60, doi: [10.1016/j.scriptamat.2015.03.006](https://doi.org/10.1016/j.scriptamat.2015.03.006).
- [46] J.C. Russ, R.T. Dehoff, *Practical Stereology*, Springer US, Boston, MA, 2000, doi: [10.1007/978-1-4615-1233-2](https://doi.org/10.1007/978-1-4615-1233-2).
- [47] E.E. Underwood, Quantitative stereology for microstructural analysis. (Eds.), in: J.L. McCall, W.M. Mueller (Eds.), *Microstructural Analysis*, Springer US, Boston, MA, 1973, pp. 35–66, doi: [10.1007/978-1-4615-8693-7_3](https://doi.org/10.1007/978-1-4615-8693-7_3).
- [48] ASM International, J.R. Davis, *ASM International, Properties and Selection: Non-ferrous Alloys and Special-Purpose Materials*, eds. ASM International, Materials Park, Ohio, 2000 [10. ed.], 6. Print.
- [49] B. Cai, X. Ma, J. Moering, H. Zhou, X. Yang, X. Zhu, Enhanced mechanical properties in Cu–Zn alloys with a gradient structure by surface mechanical attrition treatment at cryogenic temperature, *Mater. Sci. Eng. A* 626 (2015) 144–149, doi: [10.1016/j.msea.2014.12.070](https://doi.org/10.1016/j.msea.2014.12.070).
- [50] G.H. Xiao, N.R. Tao, K. Lu, Microstructures and mechanical properties of a Cu–Zn alloy subjected to cryogenic dynamic plastic deformation, *Mater. Sci. Eng. A* 513–514 (2009) 13–21, doi: [10.1016/j.msea.2009.01.022](https://doi.org/10.1016/j.msea.2009.01.022).
- [51] Y.H. Zhao, J.F. Bingert, Y.T. Zhu, X.Z. Liao, R.Z. Valiev, Z. Horita, T.G. Langdon, Y.Z. Zhou, E.J. Lavernia, Tougher ultrafine grain Cu via high-angle grain boundaries and low dislocation density, *Appl. Phys. Lett.* 92 (2008) 081903, doi: [10.1063/1.2870014](https://doi.org/10.1063/1.2870014).
- [52] D.B. Williams, C.B. Carter, *Transmission Electron Microscopy: A Textbook for Materials Science*, 2nd ed., Springer, New York, 2009.
- [53] P.M. Anderson, J.P. Hirth, J. Lothe, *Theory of Dislocations*, 2017 ed., Cambridge University Press, Cambridge, 2017 Chapter 21.
- [54] B.C. De Cooman, J. Kim, S. Lee, Heterogeneous deformation in twinning-induced plasticity steel, *Scr. Mater.* 66 (2012) 986–991, doi: [10.1016/j.scriptamat.2012.02.028](https://doi.org/10.1016/j.scriptamat.2012.02.028).
- [55] N. Hansen, Cold deformation microstructures, *Mater. Sci. Technol.* 6 (1990) 1039–1047, doi: [10.1179/mst.1990.6.11.1039](https://doi.org/10.1179/mst.1990.6.11.1039).
- [56] S.G. Chowdhury, S. Das, P.K. De, Cold rolling behaviour and textural evolution in AISI 316L austenitic stainless steel, *Acta Mater.* 53 (2005) 3951–3959, doi: [10.1016/j.actamat.2005.05.006](https://doi.org/10.1016/j.actamat.2005.05.006).
- [57] Q. Xue, X.Z. Liao, Y.T. Zhu, G.T. Gray, Formation mechanisms of nanostructures in stainless steel during high-strain-rate severe plastic deformation, *Mater. Sci. Eng. A* 410–411 (2005) 252–256, doi: [10.1016/j.msea.2005.08.022](https://doi.org/10.1016/j.msea.2005.08.022).
- [58] H. Miura, T. Sakai, S. Maruoka, J.J. Jonas, Production of recrystallized nano-grains in a fine-grained Cu–Zn alloy, *Philos. Mag. Lett.* 90 (2010) 93–101, doi: [10.1080/09500830903459648](https://doi.org/10.1080/09500830903459648).
- [59] T.J. Tiedema, W. May, W.G. Burgers, Inclusions in aluminium crystals, *Acta Crystallogr.* 2 (1949) 151–154, doi: [10.1107/S0365110X4900041](https://doi.org/10.1107/S0365110X4900041).
- [60] F. Wagner, N. Bozzolo, O. Van Landuyt, T. Grosdidier, Evolution of recrystallisation texture and microstructure in low alloyed titanium sheets, *Acta Mater.* 50 (2002) 1245–1259, doi: [10.1016/S1359-6454\(01\)00427-X](https://doi.org/10.1016/S1359-6454(01)00427-X).
- [61] V. Randle, G.S. Rohrer, Y. Hu, Five-parameter grain boundary analysis of a titanium alloy before and after low-temperature annealing, *Scr. Mater.* 58 (2008) 183–186, doi: [10.1016/j.scriptamat.2007.09.044](https://doi.org/10.1016/j.scriptamat.2007.09.044).
- [62] R.D. Doherty, D.A. Hughes, F.J. Humphreys, J.J. Jonas, D.J. Jensen, M.E. Kassner, W.E. King, T.R. McNelley, H.J. McQueen, A.D. Rollett, Current issues in recrystallization: a review, *Mater. Sci. Eng. A* 238 (1997) 219–274, doi: [10.1016/S0921-5093\(97\)00424-3](https://doi.org/10.1016/S0921-5093(97)00424-3).
- [63] N. Hansen, T. Leffers, J.K. Kjems, Recrystallization kinetics in copper investigated by *in situ* texture measurements by neutron diffraction, *Acta Metall.* 29 (1981) 1523–1533, doi: [10.1016/0001-6160\(81\)90186-3](https://doi.org/10.1016/0001-6160(81)90186-3).
- [64] G.B. Rathmayr, A. Hohenwarter, R. Pippan, Influence of grain shape and orientation on the mechanical properties of high pressure torsion deformed nickel, *Mater. Sci. Eng. A* 560 (2013) 224–231, doi: [10.1016/j.msea.2012.09.061](https://doi.org/10.1016/j.msea.2012.09.061).
- [65] G.I. Taylor, The mechanism of plastic deformation of crystals. Part I. Theoretical, *Proc. R. Soc. Math. Phys. Eng. Sci.* 145 (1934) 362–387, doi: [10.1098/rspa.1934.0106](https://doi.org/10.1098/rspa.1934.0106).
- [66] M.E. Kassner, K. Kyle, Taylor hardening in five power law creep of metals and class m alloys, *Nano and Microstructural Design of Advanced Materials*, Elsevier, 2003, pp. 255–271, doi: [10.1016/B978-008044373-7/50050-4](https://doi.org/10.1016/B978-008044373-7/50050-4).

- [67] X. Liu, F. Yuan, Y. Zhu, X. Wu, Extraordinary bauschinger effect in gradient structured copper, *Scr. Mater.* 150 (2018) 57–60, doi: [10.1016/j.scriptamat.2018.03.007](https://doi.org/10.1016/j.scriptamat.2018.03.007).
- [68] M. Yang, Y. Pan, F. Yuan, Y. Zhu, X. Wu, Back stress strengthening and strain hardening in gradient structure, *Mater. Res. Lett.* 4 (2016) 145–151, doi: [10.1080/21663831.2016.1153004](https://doi.org/10.1080/21663831.2016.1153004).
- [69] A. Misra, J.P. Hirth, R.G. Hoagland, Length-scale-dependent deformation mechanisms in incoherent metallic multilayered composites, *Acta Mater.* 53 (2005) 4817–4824, doi: [10.1016/j.actamat.2005.06.025](https://doi.org/10.1016/j.actamat.2005.06.025).
- [70] F. Kümmel, M. Kreuz, T. Hausöl, H. Höppel, M. Göken, Microstructure and mechanical properties of accumulative roll-bonded AA1050A/AA5005 laminated metal composites, *Metals* 6 (2016) 56, doi: [10.3390/met603005](https://doi.org/10.3390/met603005).
- [71] N. Hansen, Hall–Petch relation and boundary strengthening, *Scr. Mater.* 51 (2004) 801–806, doi: [10.1016/j.scriptamat.2004.06.002](https://doi.org/10.1016/j.scriptamat.2004.06.002).
- [72] J. Luster, M.A. Morris, Compatibility of deformation in two-phase Ti–Al alloys: dependence on microstructure and orientation relationships, *Metall. Mater. Trans. A* 26 (1995) 1745–1756, doi: [10.1007/BF02670762](https://doi.org/10.1007/BF02670762).